Control of photodissociation pathway for oriented adsorbed molecules using polarized light

2006 J. Phys.: Condens. Matter 18 S1345

(http://iopscience.iop.org/0953-8984/18/30/S01)

INSTITUTE OF PHYSICS PUBLISHING JOURNAL OF PHYSICS: CONDENSED MATTER

J. Phys.: Condens. Matter **18** (2006) S1345–S1356 doi:10.1088/0953-8984/18/30/S01

Control of photodissociation pathway for oriented adsorbed molecules using polarized light

E T Jensen

Physics Department, University of Northern British Columbia, 3333 University Way, Prince George, BC, V2N 4Z9, Canada

E-mail: ejensen@unbc.ca

Received 17 October 2005, in final form 23 November 2005
Published 14 July 2006
Online at stacks.iop.org/JPhysCM/18/S1345

Abstract

Molecular bilayers of CH_3X (X = Br, I) on the Cu(110)–I surface are found to have a high degree of orientational order for the C–X bond axis. This orientational order is exploited in photodissociation experiments to select different dissociative excited states on the basis of photolysis wavelength and polarization. Results are presented from the photodissociation of CH_3Br at $\lambda = 222$ and 193 nm, and CH_3I at $\lambda = 248$ and 222 nm. The Φ^* branching ratio to yield either $CH_3 + X^*(^2P_{1/2})$ or $CH_3 + X(^2P_{3/2})$ is varied between 0.06 and 0.85 depending on the molecule, wavelength and polarization selected.

1. Introduction

Various methods have been developed for the steric control of reactivity of molecules in both the gas phase and also in condensed systems. In the gas phase, molecular *orientation* has been achieved for some molecules (including CH_3I) through the use of hexapole and DC fields [1]. Molecular *alignment* has been demonstrated through the use of high $\vec{E}$ fields in a laser pulse [2]. On surfaces, much work has been done on molecules in restricted environments by exploiting the spatial [3] and orientational ordering that can occur at a surface. The goal in these works is to restrict the state of the molecules under study so that particular aspects of the molecular structure can be identified or to control the subsequent reactivity of the species.

The near-UV photodissociation of methyl halides has been studied extensively in the gas phase as well as in the adsorbed state. The gas-phase work has identified a set of low energy excitations from the ground state to repulsive excited states, dubbed the A-band. For methyl halides, the A-band consists of transitions to one of three allowed excited states which have been labelled $^3Q_1$, $^3Q_0$ and $^1Q_1$ in order of increasing energy in the Franck–Condon region. These states terminate in the formation of either $CH_3 + X(^2P_{3/2})$ or $CH_3 + X^*(^2P_{1/2})$, as shown schematically in figure 1. For X = Br the X–X* spin–orbit splitting is 0.457 eV, while for X = I the splitting is 0.943 eV. The transitions to dissociative A-band states overlap significantly, so

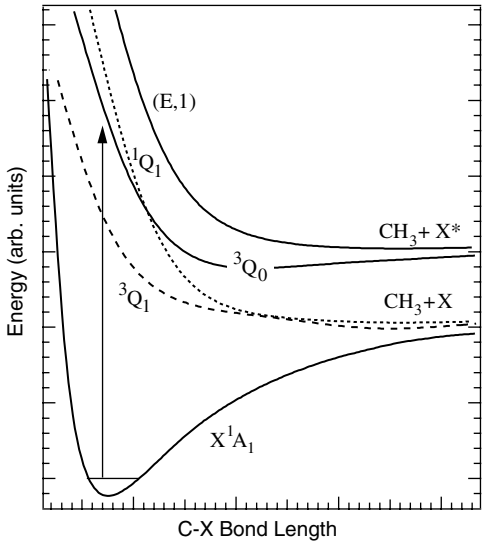

Figure 1. Schematic potential energy curves for the ground and several low-energy excited states of neutral CH_3X (X = Br, I). The A-band is generally considered to be due to transitions from the ground state to the $^3Q_1$, $^3Q_0$ and $^1Q_1$ states.

that in the gas phase the A-band appears as a single broad absorption feature. For CH_3I the A-band extends from $\lambda = 320$ to 210 nm (peaking at $\lambda = 260$ nm) [4], while for CH_3Br it extends from $\lambda = 255$ nm to beyond $\lambda = 190$ nm (peaking at $\lambda = 200$ nm) [5]. A surprising feature of the gas-phase CH_3I A-band is that the strongest absorption is $X^1A_1 - {}^3Q_0$, i.e. a singlet–triplet transition. The $X - {}^3Q_0$ dominates the $X - {}^3Q_1$ and $X - {}^1Q_1$ absorptions by a factor of about two orders of magnitude [6], with the $^3Q_1$ only significant in the long-wavelength tail of the A-band while the $^1Q_1$ makes a contribution in the short-wavelength region. The spin–orbit coupling for Br is less significant than that for I, and consequently the strengths of the $^3Q_1$ and $^1Q_1$ are more comparable to that of the $^3Q_0$ in CH_3Br photodissociation [5]. The higher energy X–(E, 1) transition shown in figure 1 is not traditionally considered in gas-phase A-band photolysis for CH_3X, but has been found to make a significant contribution in the short-wavelength A-band region for gas-phase HI [7] and for CH_3I/Cu(110)-I [8].

One way that the different transitions can be distinguished is by their transition dipoles. For excitation to the $^3Q_0$ state the transition dipole is parallel to the C–X axis, while for the $^3Q_1$ and $^1Q_1$ the transition dipoles are perpendicular to the axis. The higher-energy (E,1) transition is also a perpendicular transition. One might expect that using UV light of the appropriate wavelength polarized parallel to the C–X axis would proceed on the $^3Q_0$ potential energy surface to yield $CH_3 + X^*$ exclusively. This is not quite the case. While the absorption in this scenario would proceed via a transition to the $^3Q_0$, the $^3Q_0$–$^1Q_1$ curve crossing allows some of the dissociation to proceed via the $^1Q_1$ state, leading to the $CH_3 + X$ pathway. The probability for curve crossing has been found to be related to the fragment speed at the crossing. Molecules excited with lower photon energy (just above the crossing) pass over the crossing at low speed and have a higher probability of 'hopping' to the $^1Q_1$ than those initially excited at higher energy on the $^3Q_0$ PES. This is consistent with the picture from the Landau–Zener model [9] for this triplet–singlet transition (again, a consequence of spin–orbit coupling). Another factor in this curve crossing is the requirement that the dissociating species break C_{3v} symmetry during dissociation in order for the hopping to occur. In the case of gas-phase CH_3I, this curve crossing

has been extensively studied, while for CH_3Br somewhat less so. One measure of this process is the fraction of dissociation that proceeds via the $CH_3 + X^*$ pathway as compared to the total dissociation—the Φ^* ratio:

$$\Phi^* = \frac{(\text{Yield of } CH_3 + X^*)}{(\text{Yield of } CH_3 + X) + (\text{Yield of } CH_3 + X^*)}. \tag{1}$$

In the present work these yields in the different pathways are identified indirectly by observation of the differing translational energies of the CH_3 fragments. These translational energies are measured using a time-of-flight (TOF) technique. During photodissociation, energy is partitioned between the CH_3 and X fragments to conserve momentum, and also cause vibrational and rotational excitation of the CH_3 moiety. If it is assumed that the molecule is isolated, then the translational energy of the CH_3 fragment will be given by

$$T_{CH_3} = \left[\frac{M_X}{M_{CH_3X}}\right]\{h\nu - D_0(C - X) - E_{int}(X) - E_{int}(CH_3)\} \tag{2}$$

where M_i are the masses of the species, $h\nu$ is the photolysis energy, $D_0(C - Br) = 2.87 \pm 0.02$ eV [10], $D_0(C - I) = 2.39 \pm 0.03$ eV [6] and E_{int} are the fragment's total electronic, vibrational and/or rotational excitation energies.

In the case of A-band photodissociation of CH_3X, the bond scission is fast compared to the rotational time of the molecule. Hence, the CH_3 fragment will depart along the C–X bond axis direction and be indicative of the prior molecular orientation at the surface.

On the surface the observed fragment translational energies can be modified if the bond strength is reduced or if the species interacts significantly with the surface or co-adsorbates during or subsequent to the dissociation. For example, *chattering* in surface photodissociation has been invoked in order to explain the higher than expected translational energies for heavier fragments. In chattering, the lighter and faster moving dissociation fragment makes multiple collisions between the surface and its heavier partner, imparting larger energy to the heavier species than would be expected from a simple dissociation. A departing fragment can also interact with nearby surface sites or adsorbate molecules if the direction of the dissociation axis is aligned appropriately. This effect can be exploited for selective chemical reactivity [3, 11] if the molecular layer structure and dissociating bond direction are favourable (chemistry in a controlled geometry).

In addition to neutral photodissociation of the adsorbed molecules, we also observe dissociation due to low-energy photoelectrons. The incident UV light creates photoelectrons in the near-surface bulk region that can be transported to the surface and attach to adsorbed molecules (charge transfer, CT). This can lead to dissociation via the dissociative electron attachment (DEA) mechanism, well known from gas-phase electron–molecule scattering studies. In this CT-DEA mechanism, neutral fragments from the dissociation (in the present case CH_3) can desorb from the surface to be detected. CH_3Br and CH_3I have large DEA cross sections for very low-energy electrons [12, 13]. It is likely that subvacuum level photoelectrons are most significant in causing dissociation via CT-DEA, though for shorter UV wavelengths photoelectrons having energies above the vacuum level could also contribute.

2. Experimental details

Experiments were performed in an ultra-high-vacuum system with a base pressure in the low 10^{-10} Torr regime. The Cu(110) sample (diameter 12 mm) is mounted on a Ta plate that is suspended between sapphire plates that are in good thermal contact with the copper holder that is attached to an XYZ manipulator. The manipulator is mounted atop a differentially pumped rotary feedthrough that allows continuous rotation about the Z-axis. The sample is mounted

so that the [1$\bar{1}$0] azimuth is in the experimental scattering plane. The sample is cooled via a continuous flow of l-N_2 through the copper sample holder. The sample temperature is held fixed at ~93 K as measured by chromel–alumel thermocouples in contact with the sample. The sample is cleaned using Ar^+ ion bombardment and heating cycles. The sample cleanliness is monitored by Auger electron spectroscopy and by observation of a Cu(110) (1 × 1) LEED pattern.

The time-of-flight measurements are made with a quadrupole mass spectrometer (QMS) that is fixed on the apparatus. The QMS is located in a separately pumped section of the chamber, and is only connected to the main chamber via a 4 mm diameter aperture along the sample to the QMS ionizer line-of-sight. The QMS ionizer centre is located 203 mm from the sample, so that only a very small solid angle of desorbing neutral species from the sample can enter the QMS. Ions formed in the QMS ionizer are accelerated ($E_{\rm ion} = 25$ eV) and mass selected. The mass selected ions are then detected by an off-axis conversion dynode/electron multiplier and the pulses are amplified and fed into a multichannel scaler (MCS) for counting. In the TOF spectra presented here, a 500 ns MCS channel dwell time was used. The TOF spectra in the present work are shown corrected for the ion flight time (ionizer to multiplier) so that the flight times reflect the time of travel from the sample to the QMS ionizer.

In the present work, the dissociation is initiated by a small pulsed UV excimer laser (MPB PSX-100) operating at 248 nm (KrF), 222 nm (KrCl) and 193 nm (ArF) with unfocused 3 mm diameter ~ 5 ns pulses in the mJ per pulse energy range. The laser pulses are polarized using a birefringent MgF_2 single-crystal prism, which separates p- and s-polarized beams by ~2°. At 248 nm p- and s-polarized beams are selected by inserting and removing a zero-order half-wave plate, while for 222 and 193 nm the MgF_2 prism is rotated to select the desired beam to be incident on the sample. The axis of the incident light is fixed at 45° from the mass spectrometer axis so that as the sample is rotated to change the sample normal to the QMS angle (θ) the incident light angle ($\phi_{h\nu}$) also changes. The sample can be rotated toward the incident laser direction ($\theta > 0$, $\phi_{h\nu} < 45°$) or away from the laser ($\theta < 0$, $\phi_{h\nu} > 45°$).

Gases are adsorbed onto the cold sample by backfilling the chamber. CH_3Br gas (Aldrich 99.5%) is used as delivered and CH_3I vapour is used from room temperature liquid (Aldrich 99.5%). The gas doses corresponding to one monolayer of coverage have been determined by temperature programmed desorption experiments, supplemented by work-function change measurements [14]. It has also been observed that distinct changes in adsorbate photodissociation closely correspond to completion of the first monolayer. It is assumed that the sticking coefficient for the second and subsequent layers is similar to that of the first layer. To prepare the iodized Cu surface, roughly 2 ML of CH_3I are adsorbed on the cold surface, which is then heated. This treatment allows a dissociative thermal reaction to occur. By warming the sample to 250 °C, the CH_3(ad) dissociation product associatively desorbs [15], leaving atomic iodine on the surface. The result is a well ordered Cu(110)–I c(2 × 2) surface [14, 16].

3. Results and discussion

From submonolayer CH_3X coverages dosed onto the clean Cu(110) surface we observe that CH_3 photofragments are produced. In contrast, CH_3X submonolayers on Cu(110)–I produce essentially no detectable CH_3 photofragment signal. This observation implies that on the clean surface photodissociation of the first layer can proceed, most likely via the CT-DEA mechanism due to photoelectrons. On the Cu(110)–I surface, the requisite low-energy photoelectrons are largely suppressed. Direct photodissociation does not appear to be significant in either case, presumably due to rapid quenching of the molecular excitation due to coupling with the substrate. CT-DEA can occur in the submonolayer since this process can result in rapid

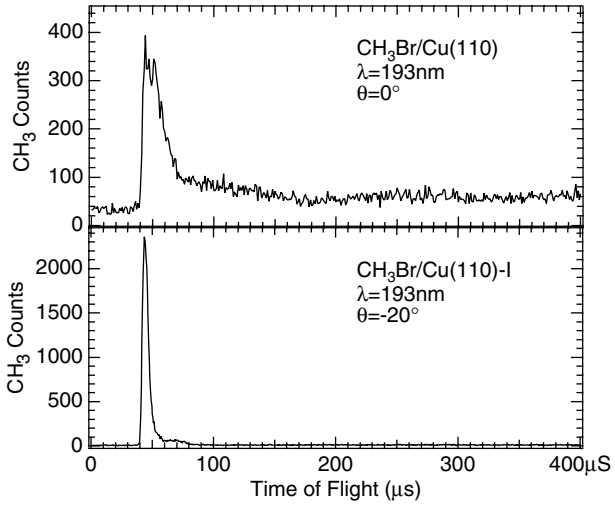

Figure 2. Time of flight spectra for 2 ML of CH_3Br adsorbed on clean Cu(110) (top) and on Cu(110)–I (bottom), both obtained using p-polarized 193 nm light. The top spectrum is obtained using 1000 laser pulses while the bottom spectrum from 500 laser pulses. For CH_3Br/Cu(110), the CH_3 yield peaks in the surface normal direction, with a broad angular distribution and wide range of arrival times. The TOF distribution for CH_3Br/Cu(110)–I is very narrow, reflecting the well defined dissociation pathways and the ordered surface structure.

bond scission that is competitive with quenching. As the CH_3X dose exceeds 1 ML, neutral photodissociation is observed on the Cu(110)–I surface and the CH_3 yield increases markedly from the CH_3X/Cu(110) surface. For the present analysis, we restrict our discussion to the case of nominal 2 ML doses on the surface.

The CH_3 time of flight spectra from 2 ML CH_3Br on clean Cu(110) are compared to that from CH_3Br/Cu(110)–I in figure 2. On Cu(110) the angular distribution is quite broad but centred around the surface normal ($\theta = 0°$). In contrast, for CH_3Br/Cu(110)–I the angular distribution is strongly peaked at $\theta = \pm 20°$ from normal. The CH_3Br/Cu(110) TOF spectrum is noticeably broader in time (i.e. a wider range of CH_3 translational energies) than for CH_3Br/Cu(110)–I. There are two main contributing factors to this broader TOF spectrum.

Firstly, on clean Cu(110), the surface barrier for low energy photoelectrons is much lower than for Cu(110)–I so that photoelectron induced reactions are relatively more important on the clean surface. These photoelectrons can reach the surface layer (charge transfer) and attach to CH_3Br and break the C–Br bond via dissociative electron attachment (CT-DEA). The CH_3 translational energy from CT-DEA is relatively insensitive to the photon energy and photoelectron energy distribution as it is generally dominated by the strong energy dependent attachment cross sections, which peak near 0 eV in the gas phase and which likely peak below the vacuum level for adsorbed CH_3Br due to image charge stabilization. The translational energies of CH_3 fragments from the CT-DEA mechanism are somewhat lower than that from direct photodissociation, resulting in a broad TOF spectrum composed of unresolved overlapping features. On the Cu(110)–I surface, the requisite low-energy photoelectrons are suppressed, so that in the case of CH_3Br the photodissociation is dominated by the direct processes. Some photodissociation from photoelectron CT-DEA can be observed, but its intensity is much reduced and the TOF feature peaks are better resolved.

A second reason for the difference in the TOF spectra of figure 2 is that the CH_3Br/Cu(110) system has significantly less orientational order than that of CH_3Br/Cu(110)–I. The less

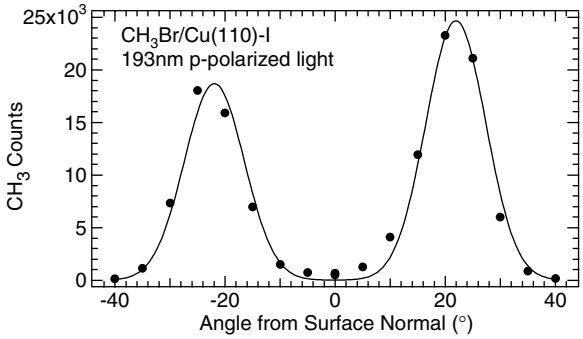

Figure 3. Angular distribution of CH_3 photofragments from 2 ML CH_3Br/Cu(110)–I obtained using p-polarized 193 nm light. Data points are obtained from individual TOF spectra using 250 laser pulses each. The data points are normalized to the signal at $\theta = +20°$ to account for the signal depletion. The distribution reflects the high degree of C–Br orientational order in the molecular layer prior to photodissociation.

ordered surface has a wider range of initial C–Br orientations, which results in a much higher likelihood of inelastic scattering between the departing CH_3 fragment and nearby adsorbate molecules and/or the surface. Similarly broadened (both in angle and in time) CH_3 TOF spectra have been observed for CH_3X (X = Br, I) on the Cu(110)–Cl surface [17], where the photoelectron yields are also suppressed but which lack the ordering observed for CH_3X/Cu(110)–I. We have also studied surface photodissociation for CH_3X adsorbed on thin alkane layers [18] in which the C–X orientation is centred on the surface normal but the distribution is narrower in angular width and where it is found that the TOF spectra also display a narrow translational energy distribution, presumably owing to a lack of significant inelastic scattering following dissociation.

The orientational ordering of CH_3Br/Cu(110)–I is demonstrated in figure 3 in which the yield of CH_3 is plotted as the sample is rotated in the $[1\bar{1}0]$ azimuth. This angular distribution is qualitatively similar to that observed from CH_3I/Cu(110)–I [14]. The measured angular distribution is shown with a fitted curve that is obtained using a function of the form $\cos^N(\theta - \theta_0)$. The best fit parameters are found to be $N = 107 \pm 8$ and $\theta_0 = 23° \pm 1°$, which is a narrower distribution than that found for CH_3I/Cu(110)–I [8] and at a slightly larger angle ($N = 65$, $\theta_0 = 21°$). In previous work on CH_3I/Cu(110)–I it was shown [14] that the distribution peaked in the $[1\bar{1}0]$ azimuth—in the [100] azimuth the CH_3 yield decreased monotonically from $\theta = 0°$. This is consistent with the results from an ESD study of CD_3I on Cu(110)–I [19]. It should also be noted that at angles other than near the peaks at $\theta = \pm 20°$, the CH_3 TOF spectra are degraded as compared to figure 2 (bottom), presumably since these 'off-angle' CH_3 photofragments have suffered inelastic interactions as they leave the surface region.

Higher resolution TOF spectra are shown for CH_3Br/Cu(110)–I in figure 4 ($\lambda = 222$ nm) and figure 5 ($\lambda = 193$ nm), and for CH_3I/Cu(110)–I in figure 6 ($\lambda = 248$ nm) and figure 7 ($\lambda = 222$ nm). In each case the figures show spectra obtained using both p-polarized light (top, $\theta = -20°$) and s-polarized light (bottom, $\theta = +20°$). For both molecules at each wavelength, the yield of CH_3 is larger from p-polarized light than from the s-polarization, though the relative amounts vary. Due to the experimental geometry, p-polarized light is incident at 45° from the C–X axis for a molecule that is 'aimed' at the QMS ionizer. If the molecule were in empty space, then equal amounts of this p-polarized light would be parallel to and perpendicular to the C–X axis. For s-polarized light, all of the incident field is perpendicular to the C–X axis.

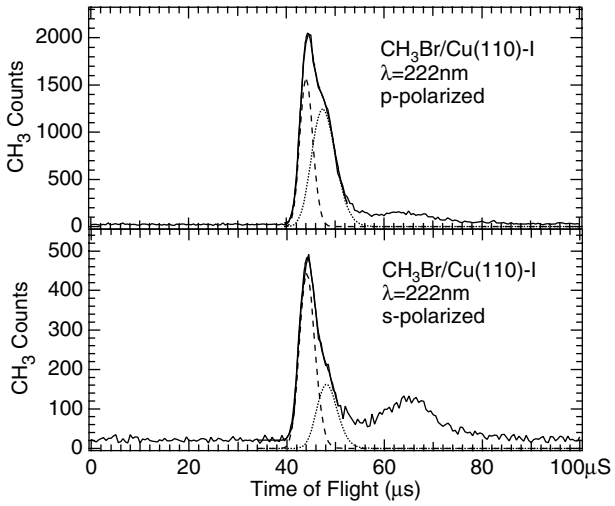

Figure 4. Time-of-flight spectra from CH_3Br/Cu(110)–I obtained at $\lambda = 222$ nm using p-polarized light (top) and s-polarized light (bottom). Also shown are fitted curves to the TOF main peak profile as discussed in the text. For the p-polarized case, the asymmetric profile is clearly composed of two peaks which reflect the main dissociation pathways. For the s-polarized TOF spectrum, the second (slower) peak is significantly reduced in intensity. The peak observed at ∼65 μs flight time is ascribed to charge-transfer dissociation.

The observation that in all cases the CH_3 yield is *reduced* for s-polarized light shows that the parallel absorption (X– $^3Q_0$) has a larger oscillator strength than the perpendicular transitions[1].

In order to extract information regarding photodissociation pathways, the TOF spectra of figures 4–7 have been fitted to a phenomenological function based on a velocity-shifted Boltzmann distribution[2]. The nonlinear fitting procedure allows for a constant background plus three parameters for each peak (intensity, streaming velocity and peak width). In several spectra, two fitted peaks are sufficient while in others a third peak is included for the cases where a significant contribution from photoelectron CT-DEA is observed (the peaks centred around 65 μs flight time). There is some difficulty in extracting reliable fits for CH_3Br/Cu(110)–I TOF spectra since the CH_3 peaks from the Br and Br* pathways overlap significantly. The true CH_3 TOF profile for a peak is not known, so the fitting procedure does not necessarily extract true peak profiles. Even without peak fitting though, it clear that for CH_3Br/Cu(110)–I at 222 nm there are substantial differences between the p- and s-polarized profiles, while at 193 nm the profiles are the same (to within experimental error).

The TOF profile from $\lambda = 222$ nm photodissociation of CH_3Br/Cu(110)–I from p-polarized light shows an asymmetrical profile that is readily decomposed into two peaks, as shown in figure 4 (top). The faster peak (centred at 41.0 μs) is from dissociation to the $CH_3 + Br$ pathway, while the peak at 44.5 μs corresponds to the $CH_3 + Br^*$ pathway. Using these fitted curves, the branching ratio is $\Phi^* \approx 0.6$. For gas-phase CH_3Br the measured $\Phi^* = 0.40$ at 222 nm, but it should be noted that this wavelength corresponds to an anomaly

[1] At the Cu surface, the p-polarized light $\vec{E}$ field components parallel to and perpendicular to the C–X axis differ, according to the Fresnel equations. In the present case, the result is that the parallel contributions are favoured to some extent, but this does not alter the basic conclusion.

[2] There is no *a priori* reason to expect that such a distribution will result in good fits, as the actual CH_3 distribution is the result of the dynamics that follow excitation to a particular state and the subsequent evolution on this potential energy surface. We have found that the fits are generally reasonable, given the small number of free parameters.

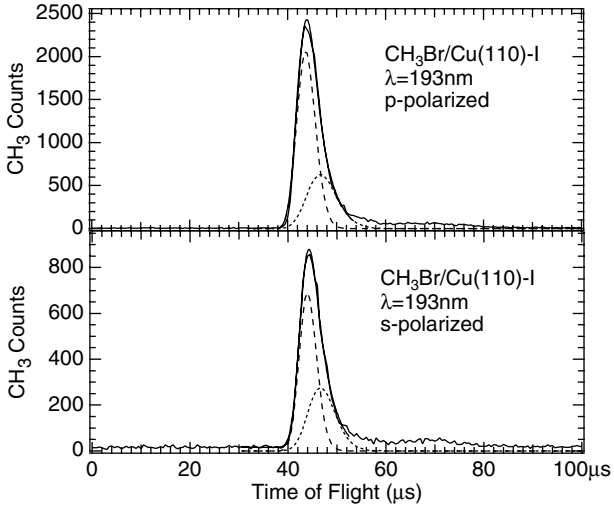

Figure 5. Time-of-flight spectra from CH_3Br/Cu(110)–I obtained at $\lambda = 193$ nm using p-polarized light (top) and s-polarized light (bottom). The TOF profiles for both polarizations are essentially identical apart from the overall intensity difference. Also shown are fitted curves to the TOF main peak profile as discussed in the text.

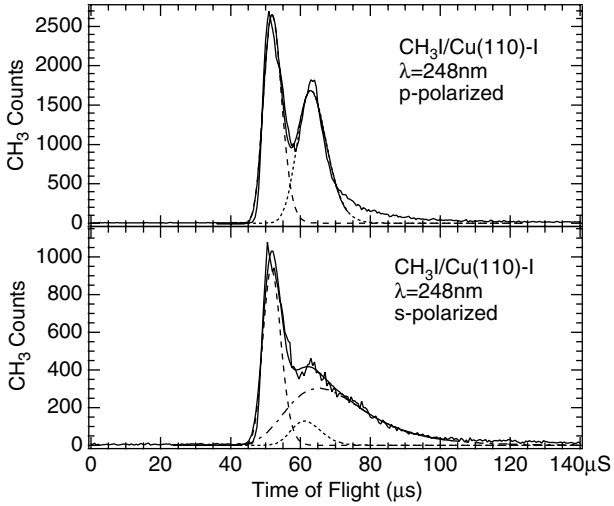

Figure 6. Time-of-flight spectra from CH_3I/Cu(110)–I obtained at $\lambda = 248$ nm using p-polarized light (top) and s-polarized light (bottom). For p-polarized light, the TOF profile is well represented by a two-peak fit. For s-polarized light, the overall CH_3 yield is much reduced and a third contribution from dissociation by photoelectrons (CT-DEA) must be included.

in which Φ^* is reduced from about 0.50 at nearby wavelengths [5]. When the incident light is switched to the s-polarization, the peak from the Br^* pathway is significantly reduced in intensity relative to the Br pathway. This is consistent with a strong parallel absorption to the $^3Q_0$ excited state for p-polarized light, while s-polarized light cannot couple to the $^3Q_0$ and so we observe the result of photodissociation from a perpendicular transition. In comparing these results to those obtained from gas-phase CH_3Br photolysis at 222 nm, it would be suspected

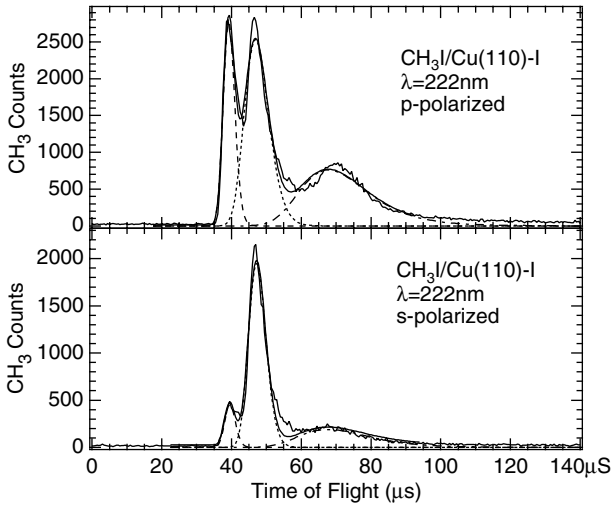

Figure 7. Time-of-flight spectra from CH_3I/Cu(110)–I obtained at $\lambda = 222$ nm using p-polarized light (top) and s-polarized light (bottom). The most significant feature in these spectra is the very low signal for the 'fast' peak in the bottom spectrum, which suggests that the relevant excited state is the (E,1). Also shown are three-peak fitted curves to the TOF main peak profile.

that the candidate perpendicular transition is to the $^3Q_1$ state, which corresponds to formation of $CH_3 + Br$ only. One question here is why for s-polarized light there is any intensity observed from the $CH_3 + Br^*$ pathway (in figure 4 bottom, $\Phi^* \approx 0.3$). One possibility is that the CH_3 TOF lineshape is inherently asymmetrical such that the 'tail' in the curve that yields the second peak in this spectrum is actually from the Br pathway. If this were the case then our estimate of the Φ^* fraction from p-polarized photodissociation would need to be reduced.

The time-of-flight spectra from CH_3Br/Cu(110)–I at 193 nm in figure 5 show a single peak, with a possible second smaller feature in the tail. Although a higher CH_3 yield is observed from p-polarized light than from s-polarized light, the TOF spectra are otherwise nearly identical, aside from the relatively larger CT-DEA contribution in the s-polarized spectra. If the main peaks in the p- and s-polarized spectra are scaled appropriately, the two spectra are indistinguishable. Fitted curves to these spectra can extract two peaks, but as in the case of the s-polarized spectrum in figure 4 (bottom) it is not clear if this second smaller peak is real or if it reflects a natural asymmetry of the $CH_3 + Br$ dissociation pathway.

If the decomposed absorption from the gas-phase CH_3Br A-band is used as a guide [5], it would be expected that the largest contribution at 193 nm would be from transition to the $^1Q_1$ state with a lesser contribution from the $^3Q_0$. If this were the case for 193 nm photodissociation of CH_3Br/Cu(110)–I, it would be expected that the yield from s-polarized light would be larger and that this would lead to exclusive dissociation to $CH_3 + Br$. P-polarized light would result in an admixture of transitions to the $^1Q_1$ and $^3Q_0$ states, resulting in TOF spectra with a more significant $CH_3 + Br*$ contribution. That the spectra in figure 5 are essentially identical is surprising. If there is significant absorption to the $^3Q_0$ state at this shorter wavelength, the curve crossing probability at the $^3Q_0$–$^1Q_1$ interface would be expected to be less significant than at 222 nm. One is forced to conclude that the excited state decomposition found for gas-phase CH_3Br near 193 nm [5] is not directly applicable to CH_3Br/Cu(110)–I.

Due to the larger spin–orbit splitting in iodine, the CH_3 TOF spectra from photodissociation of CH_3I/Cu(110)–I shows better resolution of the X and X^* dissociation pathways than for CH_3Br. In figure 6 (top) the TOF spectrum for p-polarized 248 nm light

displays a large yield of CH_3 producing a clear bimodal distribution. Switching the light to the s-polarization (figure 6 bottom) results in a much lower CH_3 yield and a significantly different CH_3 distribution. For p-polarized light, only direct photodissociation is significant and both the I and I^* dissociation pathways are prominent. The much higher CH_3 yield and the observed CH_3 distribution suggest that it is the X– $^3Q_0$ excitation that is excited by the parallel component of the incident p-polarized light. The perpendicular component is insignificant in this case, since the observed yield from s-polarized light is so much lower. Initial excitation to the $^3Q_0$ state is followed by a significant amount of curve crossing to the $^1Q_1$ to yield the observed $\Phi^* = 0.4$.

Incident s-polarized light (figure 6 bottom) has a much lower CH_3 yield so that CT-DEA is more significant in this spectrum. The largest fraction of the direct dissociation proceeds to the $CH_3 + I$ pathway. This is consistent with the perpendicular transition to the $^1Q_1$ excited state. Only a very small peak that is indicative of the $CH_3 + I^*$ pathway can be seen, the origin of which is uncertain. It is possible that a small amount of reverse curve crossing ($^1Q_1$– $^3Q_0$) is occurring, or that there is a small amount of p-polarization contamination in the incident light. It is estimated that here $\Phi^* \approx 0.06$.

For CH_3I/Cu(110)–I at the shorter wavelength of 222 nm, the p-polarized TOF spectrum of figure 7 (top) displays substantial contributions from both neutral photodissociation pathways as well as a relatively larger contribution from CT-DEA than at 248 nm. In this case, the branching ratio $\Phi^* \approx 0.61$. The large yield for the p-polarized light (again larger than for the s-polarization) and the CH_3 TOF distribution suggests that the important transition here is again the $^3Q_0$, i.e. a parallel transition moment. The higher Φ^* value at 222 nm is consistent with expectations based on the Landau–Zener model—a higher fragment velocity at the $^3Q_0$– $^1Q_1$ crossing leads to less hopping.

Using s-polarized light at 222 nm, the TOF spectrum of figure 7 (bottom) shows substantially altered dynamics, with only a very small contribution from the $CH_3 + I$ pathway. In the short-wavelength tail of the A-band, experience from gas-phase CH_3I photodissociation would suggest that the $^1Q_1$ state would be significant for perpendicular transitions [6]. However, as seen in figures 1 and 6 (bottom), dissociation via the $^1Q_1$ state results in exclusive formation of $CH_3 + I$. As discussed previously [8], the observed s-polarization TOF data at 222 nm instead requires an excited state with a perpendicular transition moment that leads to $CH_3 + I^*$. The only suitable candidate state is the (E,1) state, which has been invoked [7] in the description of HI photolysis in the short-wavelength portion of its A-band. That the observed value of Φ^* in this case is 0.85 (i.e. <1.0) suggests that there is also some contribution to the dissociation from the $^1Q_1$ state.

The dynamics of the photodissociation can also be investigated by applying equation (2) for the particular molecule and the experimental geometry. Unfortunately, the absolute arrival times for the various features have relatively large errors associated with uncertainties in the ion flight time between the ionizer and detector. Using the time *differences* between features largely eliminates these uncertainties. Using equation (2) for the X and X^* pathways gives an estimate of the time differences, ignoring differences that would arise from the internal CH_3 degrees of freedom. Variations in the time differences would arise if, during dissociation, the impulses delivered to the CH_3 fragments differ on the two pathways, leading to differences in the CH_3 vibrational excitation. Thus if the observed time difference is larger than the kinematic value it would imply that the CH_3 from the X^* pathway are slower and hence have higher internal energy, while if the observed time difference is smaller then the opposite could be surmised. Data on the time differences between the peaks from the X and X^* pathways are given in table 1.

The data of table 1 for CH_3Br at 222 and 193 nm photodissociation show only very small differences between the kinematic and observed time differences, so that it is not clear if there

Table 1. Kinematic and observed values of the time difference for CH_3 fragments between the X and X^* pathways. The time differences for CH_3Br are quite small and difficult to resolve precisely. For CH_3I, there are small but significant changes to the time differences.

Molecule	λ (nm)	$\Delta t_{\text{Kin.}}$ (μs)	$\Delta t_{\text{Obs.}}$ (μs)
CH_3Br	222	3.7	3.4(p)/3.9(s)
CH_3Br	193	2.3	2.8/2.8
CH_3I	248	9.4	10.3/11
CH_3I	222	6.3	7.2/7.2

are observable differences for the CH_3 between the two dissociation pathways. For CH_3I the observed time differences are larger for both 248 and 222 nm. The larger Δt_{Obs} values suggest that the CH_3 from the I^* pathway are hotter than those from the I pathway.

4. Summary and conclusions

The photodissociation of oriented adsorbed CH_3X (X = Br, I) molecules can be controlled by judicious choice of the dissociation wavelength and laser polarization so that particular excited states can be accessed. The photodissociation dynamics of these molecules, while displaying many of the features of the gas-phase A-band, are found to be altered in the adsorbed systems studied here. Although only three laser wavelengths were used in the present work, large differences in photodissociation dynamics were observed—for example, in CH_3I/Cu(110)–I the Φ^* branching ratio was found to vary between 0.06 and 0.85. These findings represent a new approach to work on molecular photodissociation dynamics which has some advantages over gas-phase orientation and alignment techniques, while also modifying the molecular ground and excited electronic states in the condensed phase. There is also opportunity for the application of these findings to the control of surface chemical reactivity.

Acknowledgments

The author would like to thank the Natural Sciences and Engineering Research Council (NSERC) of Canada for funding this work. Thanks also to M Lundeberg, M Stephenson and J Hnybida, who provided much assistance with these experiments as part of their NSERC Undergraduate Student Research Award tenures in the laboratory.

References

[1] Gandhi S R, Curtiss T J and Bernstein R B 1987 *Phys. Rev. Lett.* **59** 2951
[2] Stapelfeldt H and Seideman T 2003 *Rev. Mod. Phys.* **75** 543
[3] Dobrin S, Lu X, Naumkin F Y, Polanyi J C and Yang J 2004 *Surf. Sci.* **573** L363
[4] Waschewsky G C G, Horansky R and Vaida V 1996 *J. Phys. Chem.* **100** 11559
[5] Gougousi T, Samartzis P C and Kitsopoulos T N 1998 *J. Chem. Phys.* **108** 5742
[6] Eppink A T J B and Parker D H 1998 *J. Chem. Phys.* **109** 4758
[7] Le Roy R J and Kraemer G T 2002 *J. Chem. Phys.* **117** 9353
[8] Jensen E T 2005 *J. Chem. Phys.* **123** 204709
[9] Nikitin E E 1996 Adiabatic and diabatic collision processes at low energy *Atomic, Molecular, and Optical Physics Handbook* 1st edn, ed G W F Drake (New York: AIP) p 566
[10] Van Veen G N A, Baller T and De Vries A E 1985 *Chem. Phys.* **92** 59
[11] Polanyi J C and Zeiri Y 1995 Dynamics of adsorbate photochemistry *Laser Spectroscopy and Photochemistry on Metal Surfaces* ed H-L Dai and W Ho (Singapore: World Scientific) chapter 26, pp 1241–91

[12] Ayotte P, Gamache J, Bass A D, Fabrikant I I and Sanche L 1997 *J. Chem. Phys.* **106** 749
[13] Schramm A, Fabrikant I I, Weber J M, Leber E, Ruf M-W and Hotop H 1999 *J. Phys. B: At. Mol. Opt. Phys.* **32** 2153
[14] Johnson C C and Jensen E T 2000 *J. Chem. Phys.* **112** 5919
[15] Chiang C M, Wentzlaff T H and Bent B E 1992 *J. Phys. Chem.* **96** 1836
[16] Andryushechkin B V, Eltsov K N and Shevlyuga V M 2005 *Surf. Sci.* **584** 278
[17] Jensen E T, unpublished
[18] Jensen E T 2005 in preparation
[19] Lee J-G, Hong S-H, Ahner J and Yates J T Jr 2002 *Phys. Rev. Lett.* **89** 253202